

Microstructural, Wetting, and Mechanical Characteristics of Sn-57.6Bi-0.4Ag Alloys Doped with Metal-Organic Compounds

Sung-Tag Oh and Jong-Hyun Lee*

Department of Materials Science and Engineering, Seoul National University of Science and Technology,
Seoul 139-743, Korea

(received date: 15 August 2013 / accepted date: 8 January 2014 / published date: 10 March 2014)

The metallurgical and mechanical properties of the commercial low-temperature solder alloy, Sn-57.6Bi-0.4Ag (wt. %), were altered by doping with each of Pd, Co, Zn, and Ni, through reactive reflow processing by using the appropriate metal-organic compound. The use of metal-acetates resulted in appropriate doping concentrations, while the use of metal-acetylacetonates and -stearates resulted in insufficient doping concentrations. This indicates that the degree of doping is strongly dependent on the nature of the metal-organic compound used in the reactive reflow process. Notably, a concurrent decrease in the melting point and the degree of undercooling were observed only in the case of the Pd-doped alloy. In addition, the Pd-doped alloy exhibited an increase in the fraction of the primary β -Sn phase in its microstructure, and greater wettability as tested on a Cu plate. Meanwhile, the Co-doped alloy exhibited a notable increase in the size and spacing of its lamellar structure, and the Ni-doped alloy showed a refinement of its lamellar structure. Accordingly, doping with Pd and Co mitigated the brittleness of the parent Sn-57.6Bi-0.4Ag alloy, which thereby showed a pronounced increase in its plastic displacement during shear tests. Considering the increase in wettability and reduction in brittleness of the original alloy, Pd is considered to be the most suitable dopant, among all the different doping elements analyzed in this study.

Keywords: Sn-Bi-Ag alloy, doping, microstructure, wettability, mechanical properties

1. INTRODUCTION

Solders form an integral part of the semiconductor industry, and their integrity is highly essential for the reliable performance of electronic products. Of the different solder alloys used for connecting various electronic components, Pb-based alloys are the most commonly used solder materials for electronic packaging. However, the increasing environmental and health concerns over the toxicity of lead, combined with the global legislation to limit the use of Pb in manufactured products, has driven extensive research towards the development of lead-free solders. In addition, conventional high-temperature solders, which are characterized by melting temperatures above 183°C, pose several processing issues. Hence, it is highly imperative to develop environmentally friendly, low-temperature solder alloys. Given these considerations, Sn-58Bi alloy has emerged as a promising alternative, characterized by its relatively low melting point of 138°C, environmental friendliness, and economic viability.^[1-13] However, Sn-58Bi alloy has inherent limitations of low solderability when compared to other commercially available solder alloys.^[9,12,13] Moreover, Sn-58Bi alloy is brittle, especially under high-strain-rate

deformation, at which it tends to fail catastrophically by brittle fracture.^[4,9,11,14-16] These drawbacks were partially eliminated by adding small amounts of Ag to form commercially acceptable compositions such as Sn-57.6Bi-0.4Ag.^[4,9,14] Nevertheless, a comprehensive understanding of the addition of alloying/doping elements is required to further improve the mechanical properties of the alloy system.

For instance, Zerrer *et al.* demonstrated the elemental doping of a solder alloy using the reactive reflow process,^[17] wherein the metal-organic compound of the doping element was added to the Sn-3.0Ag-0.5Cu solder paste. This method is a cost-effective alloying process and can be easily applied to flux formulations for industrial applications.

Thus far, very few studies have attempted to increase the ductility and decrease the brittleness of Sn-Bi-based solder alloys.^[4,9,11,14-16,18] Similarly, not many studies have investigated the doping of Sn-Bi-Ag (SBA)-based alloys, especially with an aim to improve their mechanical properties.^[9] To this end, herein, we doped an SBA-based alloy with Pd, Co, Zn, and Ni, using the metal-organic compounds of these elements. In addition, we have systematically analyzed the effect of doping on the essential metallurgical and mechanical characteristics of the doped SBA alloys, including their melting/solidification behavior, microstructure, wettability, and mechanical properties.

*Corresponding author: pljh@snut.ac.kr
©KIM and Springer

2. EXPERIMENTAL PROCEDURE

2.1 Sample preparation

Experimental solder pastes were prepared by mixing the paste of commercial Sn-57.6Bi-0.4Ag solder alloy (ALPHA CVP-520, Cookson Electronics) with the corresponding metal-organic compound of the dopant element. The different metal-organic compounds used in this study were palladium(II) acetate (purity: 99.9%), cobalt(II) acetate (99.995%), nickel(II) acetate (97.0%), nickel(II) acetylacetonate (95.0%), zinc acetate (99.99%), and zinc stearate (91.1%). All the compounds, except zinc stearate, were purchased from Sigma-Aldrich Co., while zinc stearate was obtained from Samchun Pure Chemical Co. All the compounds were used as-received without further processing or purification. As in a typical process, 0.5 g of the metal-organic compound was mixed with 50 g of the Sn-57.6Bi-0.4Ag solder paste. In order to facilitate homogeneous mixing of the dopants with the Sn-57.6Bi-0.4Ag paste, the mixtures were blended using a homogenizer (model: Pro-200, Pro Scientific Inc.).

Subsequently, each mixture was charged in an alumina boat and reflowed using a reflow oven (model: 1809UL, Heller). The peak temperature the mixtures were subjected to was 180°C, at which they were maintained for 105 s to ensure melting. During this melting process, the metal-organic compound reacted with molten Sn-57.6Bi-0.4Ag solder paste to form an alloy. The reflow process adopted in this study is referred to as reactive reflow process for the aforementioned reasons.

2.2 Sample characterization

The doping of Sn-57.6Bi-0.4Ag alloy after the reflow process was confirmed by using inductively coupled plasma-optical emission spectroscopy (model: ICP-OES, 720-ES, Varian). The flux residues in the doped bulk specimens were washed before the ICP-OES measurements. The melting and undercooling behaviors of the doped Sn-57.6Bi-0.4Ag alloys were investigated using differential scanning calorimetry (DSC, model: Q20, TA Instruments). The microstructural and quantitative chemical analyses of the doped Sn-57.6Bi-0.4Ag alloys were performed by optical microscopy, field-emission scanning electron microscopy (FE-SEM, model: Inspect F, AP Tech Corp.), whose equipment was fitted with an energy-dispersive x-ray spectrometer (EDS, model: Silicon Drift Detector, EDAX), and electron probe microanalysis (EPMA, model: JXA-8500F, JEOL).

Subsequent to the abovementioned studies, the bulk samples of doped Sn-57.6Bi-0.4Ag alloys were melted on a pure Cu plate, using a hot plate set at 180°C. This was performed to evaluate the relative wetting areas and angles of the doped Sn-57.6Bi-0.4Ag alloys.

In order to assess the mechanical properties of the doped Sn-57.6Bi-0.4Ag alloys, the bulk alloys were made into

spherical samples of diameter 360 μm . Subsequently, the solder balls were reflowed, at a temperature profile identical to that used in the aforementioned reactive reflow process, onto organic solderability preservative (OSP)-finished pads (diameter: 500 μm) of a ball grid array (BGA) substrate. This sequence resulted in the formation of bumps of the doped Sn-57.6Bi-0.4Ag solder. The mechanical properties of these bumps were evaluated in the shear mode using a bond tester (model: Dage 4000, Dage Precision Industries). While measuring, the shearing tool was kept at a height of 100 μm from the substrate surface.

3. RESULTS AND DISCUSSION

3.1 Solidification behavior

The doping of the bulk alloy after the reactive reflow process was analyzed using ICP-OES. Table 1 summarizes the different metal-organic compounds used in this study and the corresponding amounts of doping in the bulk Sn-57.6Bi-0.4Ag alloy. As can be seen from the table, the use of metal-acetates resulted in appropriate doping concentrations, while the use of metal-acetylacetonates and -stearate resulted in insufficient doping concentrations. This indicates that metal-acetate precursors are ideal for doping the alloy. Of the two different acetate precursors used in this study, palladium(II) acetate showed strong doping capability, while that of nickel(II) acetate was relatively weak. This result suggests that the degree of doping depends on the nature of the metal-organic precursor. As the samples doped with stearate and acetylacetonate compounds did not exhibit sufficient doping concentration, they were excluded from subsequent analyses.

The heating and cooling behaviors of the Sn-57.6Bi-0.4Ag alloy and the doped alloys, as determined from their corresponding DSC thermograms, are summarized in Table 2. As can be seen from the DSC analysis, the melting onset point in the undoped reference (Sn-57.6Bi-0.4Ag) sample was around 138°C during heating.^[4,9] Intriguingly, the DSC curve of the Pd-doped Sn-57.6Bi-0.4Ag alloy exhibited distinct double solidification peaks during cooling, a behavior not observed for any of the other samples prepared in this study.

Table 1. Doping concentration of the elements in the alloys doped via the reactive reflow process, as determined from the ICP-OES analysis.

Metal-organic compound added in the process	Amount of each metal (dopant) present in the corresponding doped alloy (wt. %)
Palladium(II) acetate	0.51
Cobalt(II) acetate	0.31
Zinc acetate	0.31
Nickel(II) acetate	0.13
Zinc stearate	0.01
Nickel(II) acetylacetonate	0.06

Table 2. DSC results of the Sn-57.6Bi-0.4Ag alloys doped with various elements in different concentrations.

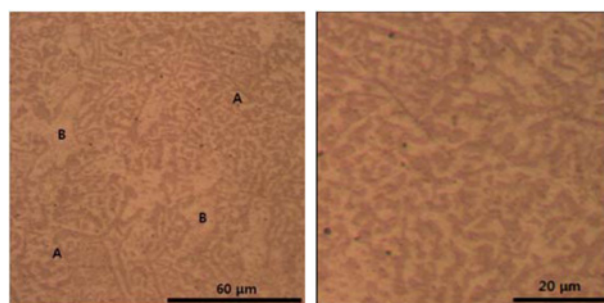
Doping conditions	Undoped (Sn-57.6Bi-0.4Ag)	Pd-doped	Co-doped	Zn-doped	Ni-doped
Onset temperature of melting (°C)	137.96	137.85	137.74	137.73	137.67
Offset temperature of melting (°C)	140.26	139.92	140.37	139.72	140.58
Onset temperature of solidification (°C)	132.40	134.09, 132.19	132.19	132.87	132.08
Offset temperature of solidification (°C)	130.65	132.26, 131.21	130.15	130.47	130.02

The appearance of the double peaks strongly implies the formation of a novel precipitate phase, in addition to the existing phases (Sn-rich, Bi-rich, and Ag_3Sn) in the alloy, during the cooling stage. Moreover, the temperature corresponding to one of the double peaks was markedly higher than that observed in the reference alloy. This indicates a decrease in the degree of undercooling.

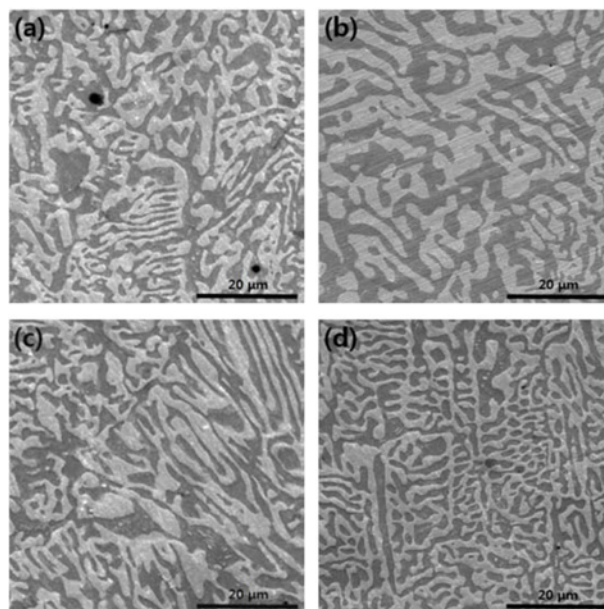
3.2 Microstructural analysis

Figure 1 shows the low- and high-magnification optical images of the undoped Sn-57.6Bi-0.4Ag alloy. Typically, the Sn-57.6Bi-0.4Ag alloy comprises a Sn-rich (solid-solution concentration of Bi = 2.7 wt. %)/Bi-rich (solid-solution concentration of Sn < 0.1 wt. %) lamellar structure, and the Ag_3Sn precipitate.^[19] However, besides the lamellar structure and the Ag_3Sn , we also observed the partial formation of primary β -Sn phases (B domains in Fig. 1; the β -Sn in lamellar structure is denoted by A domains). The formation of the primary β -Sn phase could possibly be due to the slight deviation from the eutectic composition of the Sn-57.6Bi-0.4Ag alloy and its solidification characteristics. It was also assumed that the precipitation of sparse Bi phases in the primary β -Sn phase is due to the reduction of the solid-solution content during the cooling process. The increase in the volume of the primary β -Sn phase facilitates the enhancement in the strength of the alloy, as the hardness of the Sn-rich phase tends to be much greater than that of the Bi-rich phase.^[20] The fraction of primary β -Sn phase in the undoped and doped alloys is presented in Table 3. As evidenced from the table, the fraction of primary β -Sn phase is smaller in case of Pd-, Co-, and Ni-doped alloys, when compared to that of the undoped alloy. However, this tendency did not hold true in case of the Zn-doped alloy. This, in turn, suggests the relatively poor strength of the Pd-, Co-, and Ni-doped alloys.

Figure 2 shows the microstructure of the Sn-57.6Bi-0.4Ag alloys doped with the various elements in different concentrations. As can be seen from the SEM images, the lamellar structure of the Co-doped alloy is coarser than that of the undoped Sn-57.6Bi-0.4Ag alloy, while the lamellar spacing of the Ni-doped alloy is much smaller than that of the undoped alloy. On the other hand, the lamellar spacing in case of the Pd-doped alloy is analogous to that of the undoped alloy, while that of the Zn-doped alloy is slightly

**Fig. 1.** Optical microscopic images of the undoped Sn-57.6Bi-0.4Ag alloy.**Table 3.** Fraction of the lamellar and primary β -Sn phases in each sample.

Doping conditions	Fraction of lamellar phase (%)	Fraction of primary β -Sn phase (%)
Undoped	77	23
Pd-doped	83	17
Co-doped	79	21
Zn-doped	73	27
Ni-doped	82	18

**Fig. 2.** SEM images of the Sn-57.6Bi-0.4Ag alloy doped with (a) Pd, (b) Co, (c) Zn, and (d) Ni.

higher than that of the undoped alloy. From the lamellar spacing viewpoint, it can be assumed that the doping of the solder alloy with Ni results in an increase in the strength of the alloy.

Furthermore, Fig. 3 shows the EPMA analysis of the doped Sn-57.6Bi-0.4Ag alloys, indicating the elemental distribution of each element in the alloy. Results indicate that

the doping of alloy with Pd results in the formation of coarse micron-sized precipitates of Pd-Sn. On the basis of the EDS measurements and a previously published report,^[21] these precipitates were confirmed to be PdSn₄. In addition, the microstructure of the alloy indicated the formation of submicron-sized precipitates of Ag₃Sn. The decrease in the fraction of the primary β -Sn phases, as mentioned earlier in Table 3, may be due to the fact that the Sn in the alloy is involved in the formation of PdSn₄ precipitates. Furthermore, Co doping of the alloy resulted in the formation of a solid solution in the Bi phases, and some Ag₃Sn precipitates of a size larger than a few micrometers were observed in the microstructure. Similarly, Zn doping formed a solid solution in the Bi phases, and a few micrometer-sized Ag₃Sn precipitates were formed concurrently. Likewise, the Ni doped in the alloy formed a solid solution in the Bi phases as well, and the Ag₃Sn precipitates formed in this case were submicrometer-sized particles. Based on these results, it can be concluded that the nature and amount of dopant significantly influences the microstructure of the doped Sn-57.6Bi-0.4Ag alloy, including the size of the Ag₃Sn precipitates.

3.3 Wettability characteristics

Figure 4 shows the wetting areas and angles of the doped Sn-57.6Bi-0.4Ag alloys at equilibrium, after reflowing on a Cu plate at 180°C. The wetting area of the Pd-doped Sn-57.6Bi-0.4Ag alloy was markedly greater than that of the reference (undoped) alloy. However, the wetting areas of the Co- and Zn-doped alloys were relatively smaller, whereas that of the Ni-doped alloy was even much smaller. The wetting angles exhibited a reverse trend. The wetting angle of the Pd-doped was lower, while those of the Co-, Zn-, and Ni-doped alloys were higher than that of the undoped alloy. These results show the superior wettability of the Pd-doped Sn-57.6Bi-0.4Ag alloy, which could be mainly attributed to the antioxidant nature of Pd.^[22]

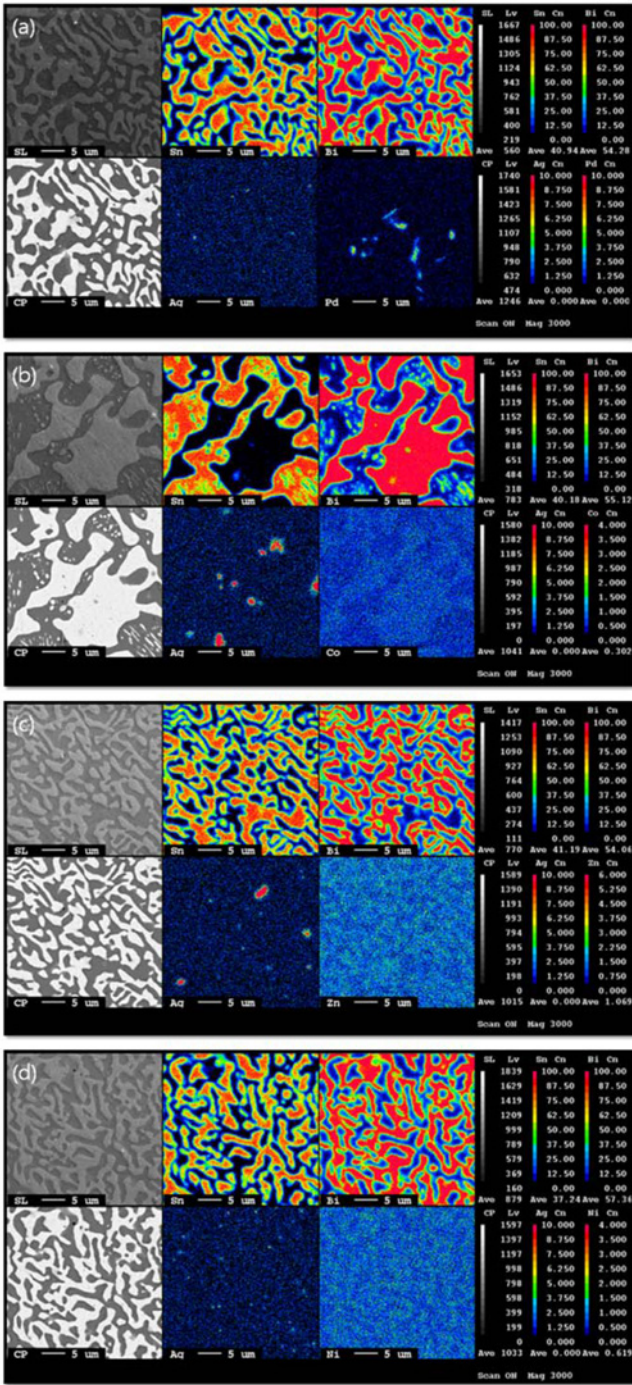


Fig. 3. EPMA results of the Sn-57.6Bi-0.4Ag alloy doped with (a) Pd, (b) Co, (c) Zn, and (d) Ni.

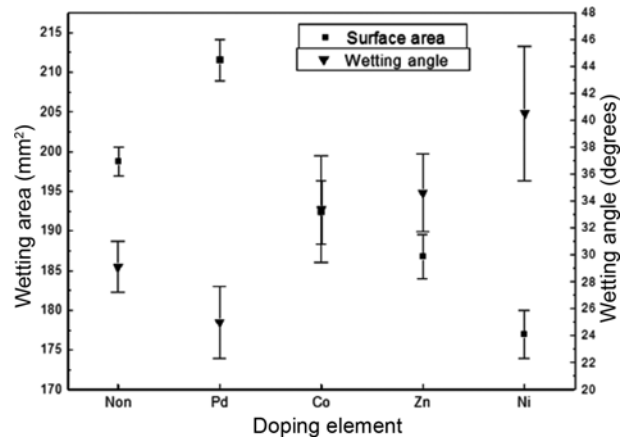


Fig. 4. Wetting areas and angles of the doped Sn-57.6Bi-0.4Ag alloys reflowed on a Cu plate at 180°C.

3.4 Mechanical properties

Figure 5 plots the maximum shear force required for shearing the doped Sn-57.6Bi-0.4Ag bumps until failure, at a rate of 250 mm/s. The shear rate and the height of shearing tool were adjusted so as to ensure that the fracture occurs within the solder bumps and not at the interface. Results indicate that the Pd- and Co-doped alloys exhibit lower shear force values than that of the undoped alloy. This could be attributed to the decrease in the fraction of the primary β -Sn phases in these alloys, and the enlarged lamellar spacing in case of the Co-doped alloy, despite the solid-solution hardening.^[11] It is assumed that the coarse PdSn₄ phases, which were irregularly distributed in the alloy, do not aid in the hardening of the precipitation. On the other hand, the Ni-doped alloy exhibited shear strength that was notably higher than that of the undoped alloy.

This could be attributed to its fine lamellar structure and solid-solution hardening, despite the decrease in the fraction of the primary β -Sn phases. Moreover, the submicron-sized Ag₃Sn precipitates were distributed uniformly in the alloy, which further contributed to the observed increase in shear strength. On the other hand, the Zn-doped alloy exhibited a slightly lower shear force value. Although an increase in the fraction of the β -Sn phases as well as solid-solution hardening were observed in the Zn-doped alloy, the slightly increased lamellar spacing and the coarsened Ag₃Sn precipitates limited the increase in its shear strength value. Based on these results, it can be surmised that the lamellar spacing and fraction of the primary β -Sn phases greatly influence the shear strength of doped Sn-57.6Bi-0.4Ag alloys.

Figure 6 shows the fracture energies of the doped Sn-57.6Bi-0.4Ag bumps at failure during the shear tests.

The displacement values until failure exhibited a trend opposite to that observed in the case of the shear force values. As a result, the Pd- and Co-doped Sn-57.6Bi-0.4Ag alloys exhibited higher fracture energy values than that of

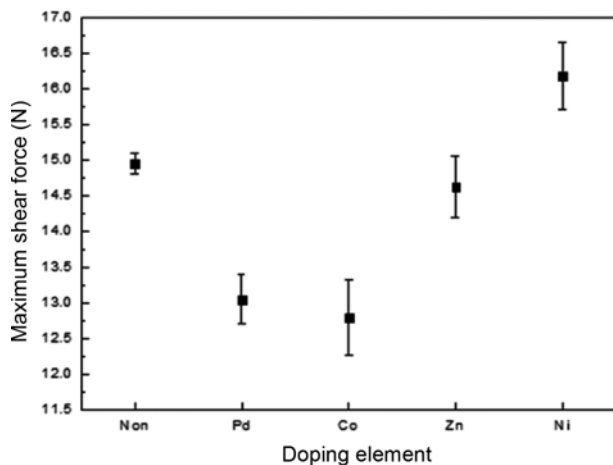


Fig. 5. Maximum shear force tolerated by the doped Sn-57.6Bi-0.4Ag alloy bumps till failure during the shear tests.

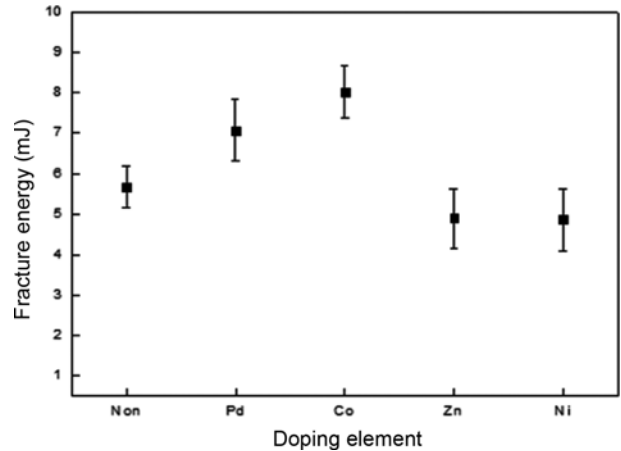


Fig. 6. Fracture energy values of the doped Sn-57.6Bi-0.4Ag alloy bumps, as determined during the shear tests.

the undoped alloy. The outstanding enhancement in the displacement accounts for the overall improvement in their fracture resistance. On the other hand, the Zn- and Ni-doped alloys exhibited fracture energy values lower than that of the undoped alloy, because of the dramatic decrease in their displacement. Consequently, co-doping Pd or Co with the existing dopant Ag could markedly reduce the brittleness of the starting alloy, which is similar to the eutectic Sn-58Bi alloy.

4. CONCLUSIONS

In summary, Sn-57.6Bi-0.4Ag alloy was successfully doped with each of Pa, Co, Zn, and Ni by mixing the corresponding metal-organic compounds of these elements to the alloy paste via the reactive reflow process. The degree of doping was found to depend on the nature of metal-organic compound used in the doping process. In case of the Pd-doped alloy, we could observe a concurrent decrease in the melting point and the degree of undercooling. Moreover, the Pd-doped alloy showed enhanced wettability on a Cu plate. On the other hand, the Co-doped alloy exhibited an increase in the size and spacing of its lamellar structure, whereas the Ni-doped alloy showed a refinement in its structures. An evaluation of the mechanical properties of the doped alloys indicates that the doping with Pd and Co markedly reduced the brittleness of the starting Sn-57.6Bi-0.4Ag alloy. Both the corresponding doped alloys exhibited a pronounced increase in elongation. Taking into account the improvement in the wettability and reduction in the brittleness of Sn-57.6Bi-0.4Ag alloy, Pd was found to be the most suitable dopant, among all the doping elements tested in the present study.

ACKNOWLEDGEMENTS

This work was financially supported by Korea Institute for Rare Metals (KIRAM).

REFERENCES

1. H. He, L. Cao, L. Wan, H. Zhao, G. Xu, and F. Guo, *Electron. Mater. Lett.* **8**, 463 (2012).
2. S. Kikuchi, M. Nishimura, K. Suetsugu, T. Ikari, and K. Matsushige, *Mater. Sci. Eng.* **A319-321**, 475 (2001).
3. H.-W. Miao and J.-G. Duh, *Mater. Chem. Phys.* **71**, 255 (2001).
4. K. Suganuma, T. Sakai, K.-S. Kim, Y. Takagi, J. Sugimoto, and M. Ueshima, *IEEE Trans. Electron., Packag., Manufac.* **25**, 257 (2002).
5. W. J. Boettinger, C. A. Handwerker, B. Newbury, T. P. Pan, and J. M. Nicholson, *J. Electron. Mater.* **31**, 545 (2002).
6. M. G. Cho, H. M. Lee, S. W. Booh, and T.-G. Kim, *J. Microelectron. Packag. Soc.* **12**, 95 (2005).
7. J. F. Li, S. H. Mannan, M. P. Clode, D. C. Whalley, and D. A. Hutt, *Acta Mater.* **52**, 2907 (2006).
8. P. J. Shang, Z. Q. Liu, D. X. Li, and J. K. Shang, *Scripta Mater.* **59**, 317 (2008).
9. W. Dong, Y. Shi, Z. Xia, Y. Lei, and F. Guo, *J. Electron. Mater.* **37**, 982 (2008).
10. H. He and G. Xu, and F. Guo, *J. Mater. Sci.* **44**, 2089 (2009).
11. Y.-Y. Shiue and T.-H. Chuang, *J. Alloy Compd.* **491**, 610 (2010).
12. M. E. Loomans, S. Vaynman, G. Ghosh, and M. E. Fine, *J. Electron. Mater.* **23**, 741 (1994).
13. T. Matsumoto and K. Nogi, *Annu. Rev. Mater. Res.* **38**, 251 (2008).
14. M. McCormack, H. S. Chen, G. W. Kammlott, and S. Jin, *J. Electron. Mater.* **26**, 954 (1997).
15. H. Takao and H. Hasegawa, *J. Electron. Mater.* **30**, 513 (2001).
16. H. Takao, A. Yamada, and H. Hasegawa, *R&D Rev. Toyota CRDL* **39**, 49 (2004).
17. P. Zerrer, A. Fix, M. Hutter, and H. Reichl, *Soldering & Surface Mount Technology* **122**, 19 (2010).
18. J.-H. Kim and J.-H. Lee, *Korean J. Met. Mater.* **49**, 211 (2011).
19. E. Çadrlıll, H. Kaya, and N. Maraşllı, *Met. Mater. Int.* **15**, 741 (2009).
20. Y. Miyazawa and T. Ariga, *Mater. Trans.* **42**, 776 (2001).
21. Y. Wang, H. K. Kim, H. K. Liou, and K. N. Tu, *Scr. Metall. Mater.* **32**, 2087 (1995).
22. C. A. Mackay and W. D. V. Voss, *Mater. Sci. Technol.* **1**, 240 (1985).